PHYSICAL REVIEW D **83,** 076002 (2011)

Exclusive $pp \to nn\pi^+\pi^+$ reaction at LHC and RHIC

P. Lebiedowicz[1,*] and A. Szczurek[2,1,†]

[1]*Institute of Nuclear Physics PAN, PL-31-342 Cracow, Poland*

[2]*University of Rzeszów, PL-35-959 Rzeszów, Poland*

(Received 25 May 2010; revised manuscript received 14 February 2011; published 1 April 2011)

We evaluate differential distributions for the four-body $pp \to nn\pi^+\pi^+$ reaction. The amplitude for the process is calculated in the Regge approach including many diagrams. We make predictions for possible future experiments at RHIC and LHC energies. Very large cross sections are found which is partially due to interference of a few mechanisms. Presence of several interfering mechanisms precludes extraction of the elastic $\pi^+\pi^+$ scattering cross section. Absorption effects are estimated. Differential distributions in pseudorapidity, rapidity, invariant two-pion mass, transverse-momentum and energy distributions of neutrons are presented for proton-proton collisions at $\sqrt{s} = 500$ GeV (RHIC) and $\sqrt{s} = 0.9$, 2.36 and 7 TeV (LHC). Cross sections with experimental cuts are presented.

DOI: 10.1103/PhysRevD.83.076002 PACS numbers: 11.55.Jy, 13.85.Lg, 14.20.Dh

I. INTRODUCTION

The total and elastic cross sections are basic objects of the scattering theory. While the proton-proton, proton-antiproton or pion-proton can be directly measured (see e.g. [1]) the pion-pion scattering is not directly accessible. It was suggested recently [2]how to extract the total $\pi^+\pi^+$ cross section in the high-energy region. Here it was suggested to use scattering of virtual π^+'s which couple to the nucleons with well known coupling constant and are subsequently promoted by the interaction onto their mass shell in the final state. The final pions are then associated with outgoing neutrons.

Can a similar method be used to extract the elastic $\pi^+\pi^+$ scattering by analysis of the $pp \to nn\pi^+\pi^+$ reaction? We wish to address this issue in the present paper.[1] The energy dependence of the total and possibly elastic cross section of pion-pion scattering would be very useful supplementary information for the groups that model hadron-hadron interactions in the soft sector (see e.g. [4]).

It was realized over the last decade that the measurement of forward particles can be an interesting and useful supplement to the central multipurpose LHC detectors (ATLAS and CMS). The main effort concentrated on the design and construction of forward proton detectors [5]. Also zero-degree calorimeters (ZDC's) have been considered as a useful supplement. It will measure very forward neutrons and photons in the pseudorapidity region $|\eta| \geq 8.5$ at the CMS[6] (see also [7]) and the ATLAS ZDC's provide coverage of the region $|\eta| \geq 8.3$ [8]. It was shown recently that the CMS (Compact Muon Spectrometer) Collaboration ZDC's provide a unique possibility to measure the $\pi^+\pi^+$ total cross section [2].

Even at high energy, the major part of the phase space of a few-body reactions is populated in soft processes which cannot be calculated within perturbative QCD. Only a limited corner of the phase space, where particles are produced at large transverse momenta, can be addressed in the framework of pQCD. At high energy, the Regge approach is the most efficient tool to describe total cross section, elastic scattering as well as different $2 \to 2$ reactions [9]. In the present paper, we shall show how to construct the amplitude for the considered $2 \to 4$ process in terms of several $2 \to 2$ soft amplitudes known from the literature. In the present analysis, we will also include absorption effects as was done recently for three-body processes [10].

In the present paper we consider an example of an exclusive reaction with two forward neutrons. Given the experimental infrastructure, the $pp \to nn\pi^+\pi^+$ is one of the reactions with four particles in the final state which could be addressed at LHC.

II. AMPLITUDE OF EXCLUSIVE $pp \to nn\pi^+\pi^+$ REACTION

A. Dominant diffractive amplitude

The diffractive mechanisms involving Pomeron and Reggeon exchanges included in the present paper are shown in Fig. 1 (with the four-momenta $p_a + p_b \to p_1 + p_2 + p_3 + p_4$). In principle, in all diagrams shown, the intermediate nucleon can be replaced by nucleon excited states. It is known that diffractive excitation of nucleons to inelastic states is rather large and constitutes about $1/3$ of the elastic scattering. This number is, however, not relevant in our case, as it is to a large extent due to the Deck type mechanism[11] which is included explicitly in our calculation. The remaining excitation to discrete nucleon states is rather small and difficult to calculate. A microscopic

*piotr.lebiedowicz@ifj.edu.pl

†antoni.szczurek@ifj.edu.pl

[1]After first version of our paper had been completed, a paper has appeared which also discusses the possibility of extraction of elastic $\pi^+\pi^+$ cross section [3]. In our analysis, we take into account many more possible mechanisms for the $pp \to nn\pi^+\pi^+$ reaction.

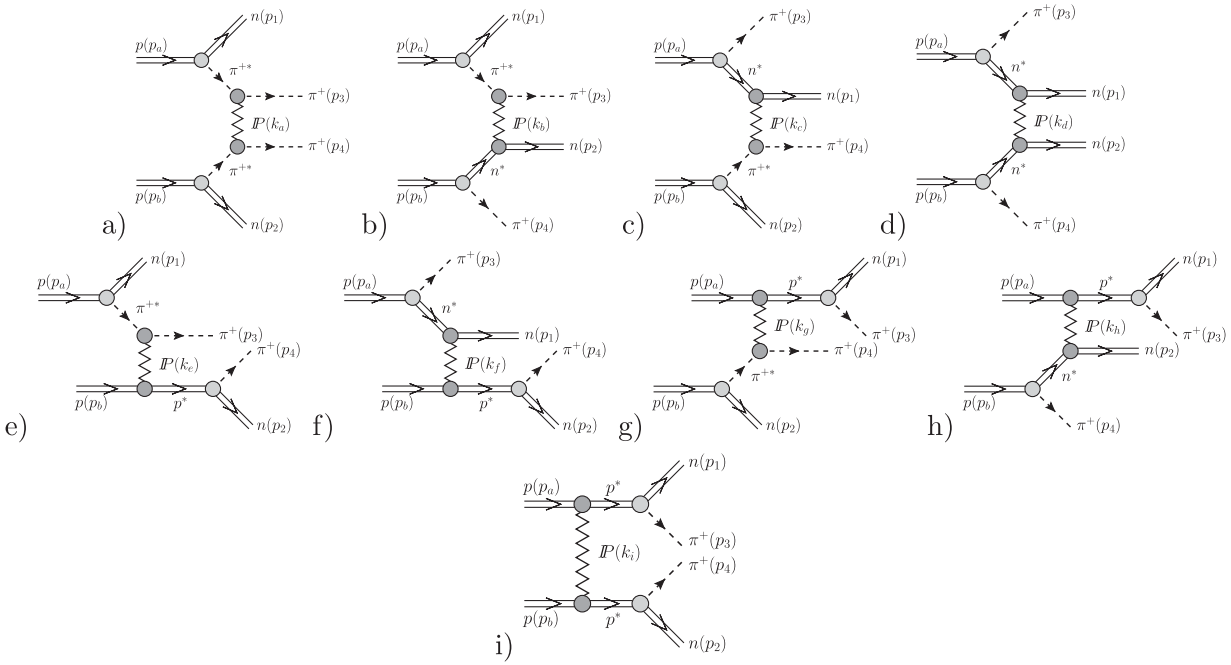

FIG. 1. Diagrams for the exclusive production of $\pi^+\pi^+$ in pp collisions at high energies. The stars attached to π^+, n and p denote the fact they are off-mass-shell. $k_a - k_i$ are four-vectors of the exchanged Pomerons.

calculation must unavoidably include not only the structure of the nucleon but also of the nucleon excited states. The cross section for $pp \to p + N\pi\pi$ of our interest is, however, only a fraction of mb [16]. That the contribution of excited discrete state is small can be also seen in the following way. First of all the diffractive transitions to discrete excited states are known to be much weaker than the elastic one. Secondly the $g_{NN^*\pi}$ coupling constants are much smaller than the $g_{NN\pi}$ coupling constant [17]. Finally the exact strength of the diffractive transitions are not known phenomenologically. Therefore in the following we neglect the contributions of diagrams with excited nucleon states.

Similarly as for the $p\bar{p} \to N\bar{N}f_0(1500)$[12] and $pp \to pp\pi^+\pi^-$ $(p\bar{p} \to p\bar{p}\pi^+\pi^-)$[21,14] reactions the amplitudes can be written in terms of Pomeron (Reggeon)-exchanges. Then the amplitude squared, averaged over the initial and summed over the final polarization states, for the $pp \to nn\pi^+\pi^+$ process can be written as:

$$\overline{|\mathcal{M}|^2} = \frac{1}{4}\sum_{\lambda_a\lambda_b\lambda_1\lambda_2} |\mathcal{M}^{(a)}_{\lambda_a\lambda_b\to\lambda_1\lambda_2} + \ldots + \mathcal{M}^{(i)}_{\lambda_a\lambda_b\to\lambda_1\lambda_2}|^2. \tag{2.1}$$

It is straightforward to evaluate the contribution shown in Fig. 1. The diagrams will be called a) – i) for brevity. If we assume the $i\gamma_5$ type coupling of the pion to the nucleon, then the Born amplitudes read[2]:

$$\begin{aligned}\mathcal{M}^{(a)}_{\lambda_a\lambda_b\to\lambda_1\lambda_2} &= \bar{u}(p_1,\lambda_1)i\gamma_5 S_\pi(t_1)u(p_a,\lambda_a)\sqrt{2}g_{\pi NN}F_{\pi NN}(t_1)\\ &\times F^{\rm off}_\pi(t_1)is_{34}C^{\pi\pi}_{IP}\left(\frac{s_{34}}{s_0}\right)^{\alpha_{IP}(k_a^2)-1}\exp\left(\frac{B_{\pi\pi}}{2}k_a^2\right)F^{off}_\pi(t_2)\\ &\times \bar{u}(p_2,\lambda_2)i\gamma_5 S_\pi(t_2)u(p_b,\lambda_b)\sqrt{2}g_{\pi NN}F_{\pi NN}(t_2),\end{aligned} \tag{2.2}$$

$$\begin{aligned}\mathcal{M}^{(b)}_{\lambda_a\lambda_b\to\lambda_1\lambda_2} &= \bar{u}(p_1,\lambda_1)i\gamma_5 S_\pi(t_1)u(p_a,\lambda_a)\sqrt{2}g_{\pi NN}F_{\pi NN}(t_1)\\ &\times F^{\rm off}_\pi(t_1)is_{23}C^{\pi N}_{IP}\left(\frac{s_{23}}{s_0}\right)^{\alpha_{IP}(k_b^2)-1}\left(\frac{s_{24}}{s_{th}}\right)^{\alpha_N(u_2)-(1/2)}\\ &\times \exp\left(\frac{B_{\pi N}}{2}k_b^2\right)F^{\rm off}_n(u_2)\times\bar{u}(p_2,\lambda_2)i\gamma_5 S_n(u_2)u(p_b,\lambda_b)\\ &\times\sqrt{2}g_{\pi NN}F_{\pi NN}(u_2),\end{aligned} \tag{2.3}$$

$$\begin{aligned}\mathcal{M}^{(c)}_{\lambda_a\lambda_b\to\lambda_1\lambda_2} &= \bar{u}(p_1,\lambda_1)i\gamma_5 S_n(u_1)u(p_a,\lambda_a)\sqrt{2}g_{\pi NN}F_{\pi NN}(u_1)\\ &\times F^{off}_n(u_1)is_{14}C^{\pi N}_{IP}\left(\frac{s_{14}}{s_0}\right)^{\alpha_{IP}(k_c^2)-1}\left(\frac{s_{13}}{s_{th}}\right)^{\alpha_N(u_1)-(1/2)}\\ &\times \exp\left(\frac{B_{\pi N}}{2}k_c^2\right)F^{off}_\pi(t_2)\times\bar{u}(p_2,\lambda_2)i\gamma_5 S_\pi(t_2)u(p_b,\lambda_b)\\ &\times\sqrt{2}g_{\pi NN}F_{\pi NN}(t_2),\end{aligned} \tag{2.4}$$

[2]We show explicitly only amplitudes for Pomeron exchange. The amplitudes for Reggeon exchange can be obtained from those for Pomeron exchange by replacing propagators by signature factors and trajectories.

$$\mathcal{M}^{(d)}_{\lambda_a\lambda_b\to\lambda_1\lambda_2} = \bar{u}(p_1,\lambda_1)\mathrm{i}\gamma_5 S_n(u_1)u(p_a,\lambda_a)\sqrt{2}g_{\pi NN}F_{\pi NN}(u_1) \times F_n^{\mathrm{off}}(u_1)\mathrm{i}s_{12}C_{IP}^{NN}\left(\frac{s_{12}}{s_0}\right)^{\alpha_{IP}(k_d^2)-1}\left(\frac{s_{13}}{s_{th}}\right)^{\alpha_N(u_1)-(1/2)} \times \left(\frac{s_{24}}{s_{th}}\right)^{\alpha_N(u_2)-(1/2)}\exp\left(\frac{B_{NN}}{2}k_d^2\right)F_n^{\mathrm{off}}(u_2) \times \bar{u}(p_2,\lambda_2)\mathrm{i}\gamma_5 S_n(u_2)u(p_b,\lambda_b)\sqrt{2}g_{\pi NN}F_{\pi NN}(u_2), \tag{2.5}$$

$$\mathcal{M}^{(e)}_{\lambda_a\lambda_b\to\lambda_1\lambda_2} = \bar{u}(p_1,\lambda_1)\mathrm{i}\gamma_5 S_\pi(t_1)u(p_a,\lambda_a)\sqrt{2}g_{\pi NN}F_{\pi NN}(t_1) \times F_\pi^{\mathrm{off}}(t_1)\mathrm{i}s_{234}C_{IP}^{\pi N}\left(\frac{s_{234}}{s_0}\right)^{\alpha_{IP}(k_e^2)-1}\exp\left(\frac{B_{\pi N}}{2}k_e^2\right)F_p^{\mathrm{off}}(s_{24}) \times \bar{u}(p_2,\lambda_2)\mathrm{i}\gamma_5 S_p(s_{24})u(p_b,\lambda_b)\sqrt{2}g_{\pi NN}F_{\pi NN}(s_{24}), \tag{2.6}$$

$$\mathcal{M}^{(f)}_{\lambda_a\lambda_b\to\lambda_1\lambda_2} = \bar{u}(p_1,\lambda_1)\mathrm{i}\gamma_5 S_n(u_1)u(p_a,\lambda_a)\sqrt{2}g_{\pi NN}F_{\pi NN}(u_1) \times F_n^{\mathrm{off}}(u_1)\mathrm{i}s_{124}C_{IP}^{NN}\left(\frac{s_{124}}{s_0}\right)^{\alpha_{IP}(k_f^2)-1}\left(\frac{s_{13}}{s_{th}}\right)^{\alpha_N(u_1)-(1/2)} \times \exp\left(\frac{B_{NN}}{2}k_f^2\right)F_p^{\mathrm{off}}(s_{24}) \times \bar{u}(p_2,\lambda_2)\mathrm{i}\gamma_5 S_p(s_{24})u(p_b,\lambda_b) \times \sqrt{2}g_{\pi NN}F_{\pi NN}(s_{24}), \tag{2.7}$$

$$\mathcal{M}^{(g)}_{\lambda_a\lambda_b\to\lambda_1\lambda_2} = \bar{u}(p_1,\lambda_1)\mathrm{i}\gamma_5 S_p(s_{13})u(p_a,\lambda_a)\sqrt{2}g_{\pi NN}F_{\pi NN}(s_{13}) \times F_p^{off}(s_{13})\mathrm{i}s_{134}C_{IP}^{\pi N}\left(\frac{s_{134}}{s_0}\right)^{\alpha_{IP}(k_g^2)-1}\exp\left(\frac{B_{\pi N}}{2}k_g^2\right)F_\pi^{\mathrm{off}}(t_2) \times \bar{u}(p_2,\lambda_2)\mathrm{i}\gamma_5 S_\pi(t_2)u(p_b,\lambda_b)\sqrt{2}g_{\pi NN}F_{\pi NN}(t_2), \tag{2.8}$$

$$\mathcal{M}^{(h)}_{\lambda_a\lambda_b\to\lambda_1\lambda_2} = \bar{u}(p_1,\lambda_1)\mathrm{i}\gamma_5 S_p(s_{13})u(p_a,\lambda_a)\sqrt{2}g_{\pi NN}F_{\pi NN}(s_{13}) \times F_p^{off}(s_{13})\mathrm{i}s_{123}C_{IP}^{NN}\left(\frac{s_{123}}{s_0}\right)^{\alpha_{IP}(k_h^2)-1}\left(\frac{s_{24}}{s_{th}}\right)^{\alpha_N(u_2)-(1/2)} \times \exp\left(\frac{B_{NN}}{2}k_h^2\right)F_n^{\mathrm{off}}(u_2)\bar{u}(p_2,\lambda_2)\mathrm{i}\gamma_5 S_n(u_2)u(p_b,\lambda_b) \times \sqrt{2}g_{\pi NN}F_{\pi NN}(u_2), \tag{2.9}$$

$$\mathcal{M}^{(i)}_{\lambda_a\lambda_b\to\lambda_1\lambda_2} = \bar{u}(p_1,\lambda_1)\mathrm{i}\gamma_5 S_p(s_{13})u(p_a,\lambda_a)\sqrt{2}g_{\pi NN}F_{\pi NN}(s_{13}) \times F_p^{\mathrm{off}}(s_{13})\mathrm{i}s_{ab}C_{IP}^{NN}\left(\frac{s_{ab}}{s_0}\right)^{\alpha_{IP}(k_i^2)-1}\exp\left(\frac{B_{NN}}{2}k_i^2\right)F_p^{\mathrm{off}}(s_{24}) \times \bar{u}(p_2,\lambda_2)\mathrm{i}\gamma_5 S_p(s_{24})u(p_b,\lambda_b)\sqrt{2}g_{\pi NN}F_{\pi NN}(s_{24}), \tag{2.10}$$

where the energy scale s_0 is fixed at $s_0 = 1\ \mathrm{GeV}^2$ and $s_{\mathrm{th}} = (m_N + m_\pi)^2$.

In the above equations $u(p_i,\lambda_i)$, $\bar{u}(p_f,\lambda_f) = u^\dagger(p_f,\lambda_f)\gamma^0$ are the Dirac spinors (normalized as $\bar{u}(p)u(p) = 2m_N$) of the initial protons and outgoing neutrons with the four-momentum p and the helicities of the nucleons λ. The propagators of virtual particles can be written as

$$S_\pi(t_{1,2}) = \frac{\mathrm{i}}{t_{1,2} - m_\pi^2}, \tag{2.11}$$

$$S_n(u_{1,2}) = \frac{\mathrm{i}(\tilde{u}_{1,2_\nu}\gamma^\nu + m_n)}{u_{1,2} - m_n^2}, \tag{2.12}$$

$$S_p(s_{ij}) = \frac{\mathrm{i}(\tilde{s}_{ij_\nu}\gamma^\nu + m_p)}{s_{ij} - m_p^2}, \tag{2.13}$$

where $t_{1,2} = (p_{a,b} - p_{1,2})^2$ and $u_{1,2} = (p_{a,b} - p_{3,4})^2 = \tilde{u}_{1,2}^2$ are the four-momenta squared of transferred pions and neutrons, respectively.[3] $s_{ij} = (p_i + p_j)^2 = \tilde{s}_{ij}^2$ are the squared invariant masses of the (i, j) system, m_π and m_n, m_p are the pion and nucleons masses, respectively. The factor $g_{\pi NN}$ is the pion nucleon coupling constant, which is relatively well known[15] ($g_{\pi NN}^2/4\pi = 13.5$–14.6). In our calculations, the coupling constant is taken as $g_{\pi NN}^2/4\pi = 13.5$.

Using the known strength parameters for the NN and πN scattering fitted to the corresponding total cross sections (the Donnachie-Landshoff model [18]), we obtain C_{IP}^{NN}, $C_{IP}^{\pi N}$ and assuming Regge factorization $C_{IP}^{\pi\pi}$. The Pomeron/Reggeon trajectories determined from elastic and total cross sections are given in the linear approximation[4] ($\alpha_i(t) = \alpha_i(0) + \alpha_i' t$) where the values of relevant parameters (the intercept $\alpha_i(0)$ and the slope of trajectory α_i' in GeV^{-2}) are also taken from the Donnachie-Landshoff model for consistency. Parameters of Reggeon exchanges used in the present calculations are listed in Table I.

[3] In the following, for brevity we shall use notation $t_{1,2}$ which means t_1 or t_2.

[4] For simplicity we use the linear Pomeron/Reggeons' trajectories, but further improvements are possible.

TABLE I. Parameters of Reggeon exchanges used in the present calculations.

i	η_i	$\alpha_i(t)$	C_i^{NN} (mb)	$C_i^{\pi N}$ (mb)	$C_i^{\pi\pi}$ (mb)	r_T^i
IP	i	$1.0808 + (0.25\ \mathrm{GeV}^{-2})t$	21.7	13.63	8.56	—
f_2	$(-0.860895 + \mathrm{i})$	$0.5475 + (0.93\ \mathrm{GeV}^{-2})t$	75.4875	31.79	$\simeq 13.39$	—
ρ	$(-1.16158 - \mathrm{i})$	$0.5475 + (0.93\ \mathrm{GeV}^{-2})t$	1.0925	4.23	$\simeq 16.38$	7.5
a_2	$(-1 + \mathrm{i})$	$0.5 + (0.9\ \mathrm{GeV}^{-2})t$	1.7475	—	—	6
ω	$(-1 - \mathrm{i})$	$0.5 + (0.9\ \mathrm{GeV}^{-2})t$	20.0625	—	—	0

The slope parameter can be written as

$$B(s) = B_0 + 2\alpha'_{IP} \ln\left(\frac{s}{s_0}\right), \tag{2.14}$$

where B_0 is the t-slope of the elastic differential cross section. In our calculation, we use B_0: $B_{\pi N} = 6.5\ \mathrm{GeV}^{-2}$, $B_{NN} = 9\ \mathrm{GeV}^{-2}$ and $B_{\pi\pi} = 4\ \mathrm{GeV}^{-2}$. The value of $B_{\pi\pi}$ is not well known, however the Regge factorization entails $B_{\pi\pi} \approx 2B_{\pi N} - B_{NN}$ [13]. We have parametrized the $k_a^2, \ldots, k_i^2$ dependences in the exponential form (see formulas (2.2), (2.3), (2.4), (2.5), (2.6), (2.7), (2.8), (2.9), and (2.10)).

We improve the parametrization of the amplitudes for neutron exchange (2.3), (2.4), (2.5), (2.7), and (2.9), by the factors $(\frac{s_{ij}}{s_{th}})^{\alpha_N(u_{1,2})-(1/2)}$ to reproduce the high-energy Regge dependence. The degenerate nucleon trajectory is $\alpha_N(u_{1,2}) = -0.3 + \alpha'_N u_{1,2}$, with $\alpha'_N = 0.9\ \mathrm{GeV}^{-2}$.

The extra correction factors $F^{off}_{\pi,N}(k^2)$ (where $k^2 = t_{1,2}, u_{1,2}, s_{ij}$) are due to off-shellness of particles. In the case of our four-body reaction rather large transferred four-momenta squared k^2 are involved and one has to include the non-point-like and off-shellness nature of the particles involved in corresponding vertices. This is incorporated via $F_{\pi NN}(k^2)$ vertex form factors. We parametrize these form factors in the following exponential form:

$$F(t_{1,2}) = \exp\left(\frac{t_{1,2} - m_\pi^2}{\Lambda^2}\right), \tag{2.15}$$

$$F(u_{1,2}) = \exp\left(\frac{u_{1,2} - m_n^2}{\Lambda^2}\right), \tag{2.16}$$

$$F(s_{ij}) = \exp\left(\frac{-(s_{ij} - m_p^2)}{\Lambda^2}\right). \tag{2.17}$$

While four-momenta squared of transferred pions $t_{1,2} < 0$, it is not the case for transferred neutrons where $u_{1,2} < m_n^2$. In general, the cutoff parameter Λ_{off} is not known but in principle could be fitted to the (normalized) experimental data. From our general experience in hadronic physics we expect $\Lambda_{\mathrm{off}} \sim 1$ GeV. Typical values of the πNN form factor parameters used in the meson exchange models are $\Lambda = 1.2$–1.4 GeV [19], however the Gottfried sum fule violation prefers smaller $\Lambda \approx 0.8$ GeV [20]. In our calculation, if not otherwise mentioned, we use $\Lambda = \Lambda_{\mathrm{off}} = 1$ GeV. We shall discuss how uncertainties of the form factors influence our final results.

B. Single and double charge exchanges with subleading Reggeons ρ^+, a_2^+

We wish to include also specific processes with isovector Reggeon exchanges. We include processes shown in Fig. 2. These processes involve $\rho^+\rho^+ \to \pi^+\pi^+$ and $a_2^+ a_2^+ \to \pi^+\pi^+$ subprocesses. Unfortunately these subprocesses (or the reverse ones) could not be studied experimentally.

The relevant coupling constants in the diagrams in Figs. 2(b) and 2(c) are not known and cannot be obtained from first principles, therefore one has to refer to other reactions involving the same coupling constants. Such reactions are e.g. $\pi^\pm p \to a_2^\pm p$ (where both $IP \mp \rho^0$ exchanges are possible), $\pi^- p \to a_2^0 n$, $\pi^- p \to \omega^0 n$ (only ρ^+-Reggeon exchange come into play), $\pi^\pm p \to \rho^\pm p$ (π^0, ω^0- and a_2^0-Reggeon exchanges) and $\pi^- p \to \rho^0 n$ (π^+, a_2^+-Reggeon exchanges). The details of how to fix parameters of these two-body reactions are described in the Appendix.

The diagram in Fig. 2(a) is topologically identical to the dominant diagram for the $pp \to pp\pi^+\pi^-$ reaction [21]. There, however, the Pomeron-Pomeron, Pomeron-Reggeon and Reggeon-Pomeron exchanges are the dominant processes. In addition to Fig. 2(a), there is possibly also another mechanism with the intermediate pion replaced by a virtual photon. Because it requires two electromagnetic couplings instead of two strong couplings, its contribution should be small. Because of the extra photon propagator, it could be enhanced when $k_\gamma^2 \to 0$. However, then the vertices should tend to zero. Therefore we can safely omit such a diagram.

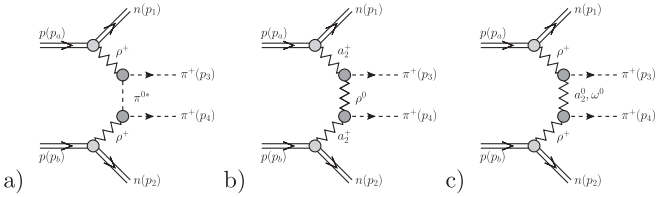

FIG. 2. Diagrams with subleading-charged Reggeon exchanges in pp collisions at high energies.

We write the amplitudes for the diagrams in Fig. 2 as

$$\mathcal{M}_{\lambda_a\lambda_b\to\lambda_1\lambda_2} = \sqrt{2}\left(\frac{-t_1}{4m_N^2}\right)^{|\lambda_1-\lambda_a|/2} r_T^{i|\lambda_1-\lambda_a|}\eta_{IR}s_{13} \times\sqrt{C_{IR}^{NN}}\left(\frac{s_{13}}{s_0}\right)^{\alpha_{IR}(t_1)-1}\exp\left(\frac{B_{MN}}{2}t_1\right)\mathcal{A}(s_{34},t_a) \times\sqrt{2}\left(\frac{-t_2}{4m_N^2}\right)^{|\lambda_2-\lambda_b|/2} r_T^{i|\lambda_2-\lambda_b|}\eta_{IR}s_{24} \times\sqrt{C_{IR}^{NN}}\left(\frac{s_{24}}{s_0}\right)^{\alpha_{IR}(t_2)-1}\exp\left(\frac{B_{MN}}{2}t_2\right) + \text{crossed term}, \quad (2.18)$$

where $\mathcal{A}(s_{34}, t_a)$ refers to the central part of the diagrams

$$\mathcal{A}^{\pi-\text{exch.}}(s_{34}, t_a) = F_\pi^{\text{off}}(t_a)\sqrt{C_\rho^{\pi\pi}}\frac{1}{t_a - m_\pi^2}\sqrt{C_\rho^{\pi\pi}}F_\pi^{\text{off}}(t_a), \quad (2.19)$$

$$\mathcal{A}^{\text{Reggeon}-\text{exch.}}(s_{34}, t_a) = \frac{\sqrt{-t_a}}{M_0}\eta_i s_{34}(g^i_{j\to\pi})^2\left(\frac{s_{34}}{s_0}\right)^{\alpha_i(t_a)-1} \times\exp\left(\frac{B_{MM}}{2}t_a\right)\frac{\sqrt{-t_a}}{M_0}. \quad (2.20)$$

In actual calculations, we take $B_{MN} = B_{\pi N}$ and $B_{MM} = B_{\pi\pi}$. Since, in the diagrams in Fig. 2 and 3, we have Reggeon exchanges rather than meson exchanges, formulas (2.18) and (2.20) give rather the upper limits for the cross section.

The parametrization of the amplitudes with subleading-charged Reggeon exchanges cannot be used in the region of resonances in πN or/and $\pi\pi$ subsystems [21]. Therefore, the amplitude used in the calculations must contain restrictions on the four-body phase space. To exclude the regions of resonances, we modify the parametrization of the amplitudes by multiplying cross section by a purely phenomenological smooth cutoff correction factor (see [21]):

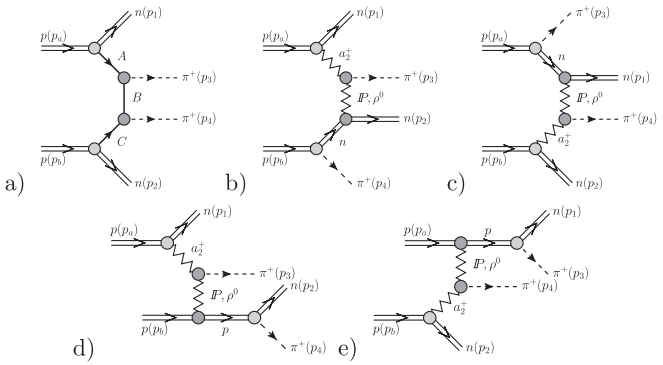

FIG. 3. Diagrams with subleading Reggeon a_2^+ exchange in pp collisions at high energies.

TABLE II. Different realizations of the diagram in Fig. 3(a).

A	a_2^+	a_2^+	π^+	a_2^+	π^+
B	IP	IP	IP	ρ^0	ρ^0
C	a_2^+	π^+	a_2^+	π^+	a_2^+

$$f_{\text{cont}}^{\pi N/\pi\pi}(W_{\pi N/\pi\pi}) = \frac{\exp\left(\frac{W-W_0}{a}\right)}{1+\exp\left(\frac{W-W_0}{a}\right)}. \quad (2.21)$$

The parameter W_0 gives the position of the cut and the parameter a describes how sharp is the cutoff. For large energies $f_{\text{cont}}^{\pi N/\pi\pi}(W_{\pi N/\pi\pi}) \approx 1$ and close to kinematical threshold $f_{\text{cont}}^{\pi N/\pi\pi}(W_{\pi N/\pi\pi}) \approx 0$. In our calculation we take $W_0 = 2$ GeV and $a = 0.2$ GeV.

There is another class of diagrams shown in Fig. 3. The diagram in Fig. 3(a) represents a generic amplitude, with particle sets (A, B, C) collected in Table II. In contrast to the diagrams shown in Fig. 2, here both pions and subleading Reggeons couple to nucleons. We shall not present explicit formulas for the corresponding amplitudes here. We shall show separate contributions of those processes in Sec III.

C. Absorptive corrections

The absorptive corrections in Fig. 4 are calculated as described for the three-body processes[10]. Here the absorptive correction to the bare amplitude (see Fig. 1) can be written as

$$\delta\mathcal{M}_{\lambda_a\lambda_b\to\lambda_1\lambda_2}(\vec{p}_{1t}, \vec{p}_{2t}) = i\int\frac{d^2k_t}{8\pi^2}\frac{T(s,k_t^2)}{s}\mathcal{M}^{(0)}_{\lambda_a\lambda_b\to\lambda_1\lambda_2} \times(\vec{p}^{\,*}_{at} - \vec{p}_{1t}, \vec{p}^{\,*}_{bt} - \vec{p}_{2t}), \quad (2.22)$$

where $p_a^* = p_a - k_t$, $p_b^* = p_b + k_t$ with momentum transfer k_t. Above $\mathcal{M}^{(0)}_{\lambda_a\lambda_b\to\lambda_1\lambda_2}$ is a bare amplitude calculated as described in the previous subsections. $T(s, k_t^2)$ is an elastic proton-proton amplitude for the appropriate energy. It can be conveniently parametrized as

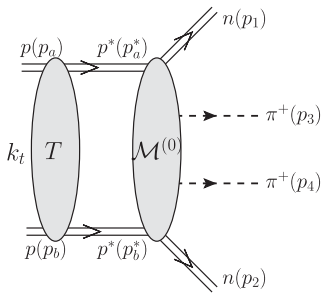

FIG. 4. Schematic diagram for absorption effects due to proton-proton interaction.

TABLE III. Full-phase-space integrated cross section (in mb) for exclusive $nn\pi^+\pi^+$ production at selected center-of-mass energies and different values of the form factor parameters. In parentheses, we show cross sections including absorption effects.

	$W = 0.5$ TeV	$W = 0.9$ TeV	$W = 2.36$ TeV	$W = 7$ TeV
$\Lambda = 0.8$ GeV, $\Lambda_{\rm off} = 1$ GeV	0.34 (0.15)	0.38 (0.16)	0.47 (0.18)	0.59 (0.19)
$\Lambda = \Lambda_{\rm off} = 1$ GeV	0.84 (0.37)	0.95 (0.39)	1.16 (0.42)	1.47 (0.46)
$\Lambda = 1.2$ GeV, $\Lambda_{\rm off} = 1$ GeV	1.45 (0.62)	1.64 (0.66)	2.01 (0.71)	2.55 (0.77)

$$T(s, k_t^2) = A_0(s)\exp(-B_{NN}k_t^2/2). \tag{2.23}$$

From the optical theorem we have $\mathrm{Im}A_0(s) = s\sigma_{\rm tot}^{pp}(s)$ (the real part is small in the high-energy limit). Again the Donnachie-Landshoff parametrization of the total pp or $p\bar{p}$ cross sections can be used to calculate the rescattering amplitude.

In our analysis, the $\pi^+ n$ interactions are not taken into account. They would further decrease the cross section. Given other theoretical uncertainties (form factors), it seems not worthwhile to take over the effort of performing very time-consuming calculations. Absorption effects for exclusive Higgs production are discussed e.g. in Ref. [22].

The cross section is obtained by assuming a general $2 \to 4$ reaction

$$\sigma = \int \frac{1}{2s}\overline{|\mathcal{M}|^2}(2\pi)^4\delta^4(p_a + p_b - p_1 - p_2 - p_3 - p_4) \times \frac{d^3p_1}{(2\pi)^3 2E_1}\frac{d^3p_2}{(2\pi)^3 2E_2}\frac{d^3p_3}{(2\pi)^3 2E_3}\frac{d^3p_4}{(2\pi)^3 2E_4}. \tag{2.24}$$

To calculate the total cross section, one has to calculate 8-dimensional integral numerically. The details of how to conveniently reduce the number of kinematical integration variables are given elsewhere [21].

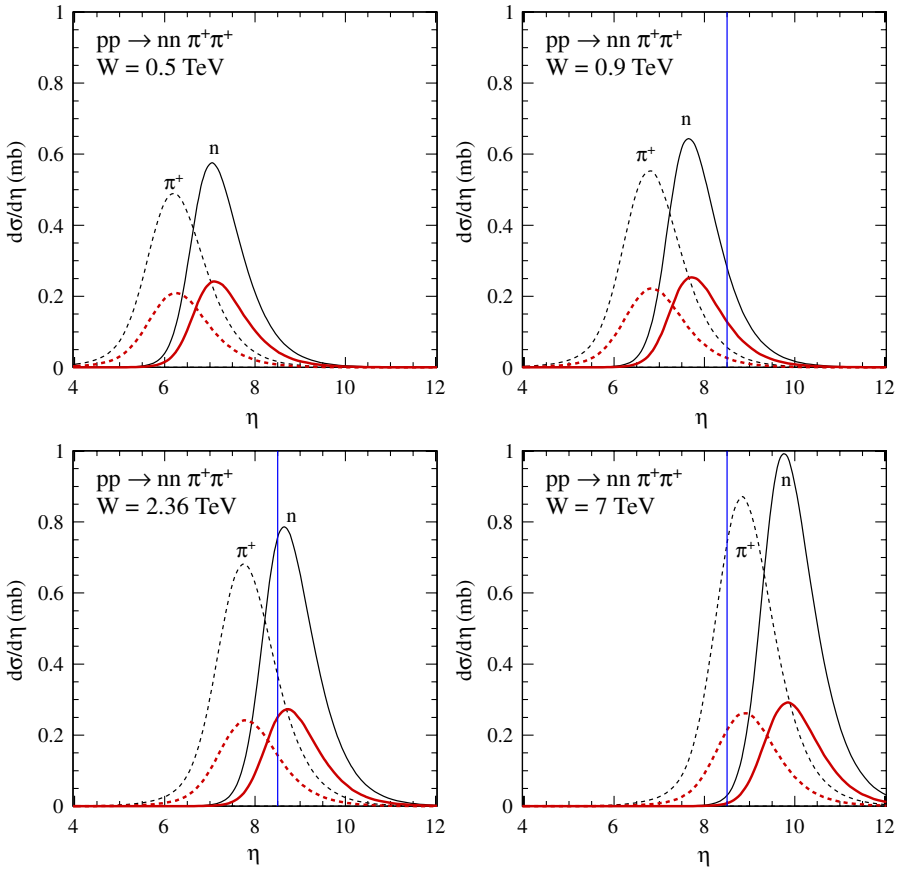

FIG. 5 (color online). Differential cross section $d\sigma/d\eta$ for neutrons (solid lines) and pions (dotted lines) at the center-of-mass energies $W = 0.5, 0.9, 2.36, 7$ TeV. The smaller bumps include absorption effects calculated in a way described in Sec. II C. In this calculation, we have used $\Lambda = \Lambda_{\rm off} = 1$ GeV. The vertical lines at $\eta = \pm 8.5$ are the lower limits of the CMS ZDC's. The details about RHIC ZDC's can be found in Ref. [25].

III. RESULTS

We shall show our predictions for the $pp \to nn\pi^+\pi^+$ reaction for several differential distributions in different variables at selected center-of-mass energies $W = 500$ GeV (RHIC) and $W = 0.9$, 2.36 and 7 TeV (LHC). The cross section slowly rises with incident energy. In general, the higher the energy, the higher the absorption effects. The results depend on the value of the nonperturbative, *a priori* unknown parameter of the form factor responsible for off-shell effects. In Table III, we have collected integrated cross sections for selected energies and different values of the model parameters. We show how the uncertainties of the form factor parameters affect our final results.

In Fig. 5, we show distributions in pseudorapidity ($\eta = -\ln(\tan\frac{\theta}{2})$, where θ is the angle between the particle momentum and the beam axis) for the $pp \to nn\pi^+\pi^+$ reaction. The discussed reaction is very unique because not only neutrons but also pions are produced dominantly in very forward or very background directions, forming a large size gap in pseudorapidity between the produced pions, about 12 units at $W = 7$ TeV. While neutrons can be measured by the ZDC's, the measurement of very forward/backward pions requires further studies. A possible evidence of the reaction discussed here is a signal from both ZDC's and no signal in the central detector.

In Fig. 6 we present rapidity distributions of pions y_{π^+} and rapidity distributions of neutrons y_n. Please note a very limited range of rapidities shown in the figure. The contributions for individual diagrams a)—i) (see Fig. 1) are also shown. The diagram in Fig. 1(d) gives the largest contribution. One can observe specific symmetries between different contributions on the left and right panels. For instance, the long-dash-dotted line on the left panel (corresponding to the diagram in Fig. 1(b)) is symmetric to the dashed line on the right panel (corresponding to the diagram in Fig. 1(c)). Clearly, a significant interference effect can be seen. There is no region of either pion or neutron rapidity where the diagram (a) dominates. This makes the possibility of extracting of $\pi^+\pi^+$ elastic scattering very difficult.

For completeness, in Fig. 7 we show the contribution of the diagrams with subleading-charged Reggeon exchanges (see Fig. 2), which could not be seen in the previous plot. We show results for the RHIC (left panel) and LHC (right panel) energies. In contrast to the other mechanisms, the corresponding contribution is rather flat over broad range

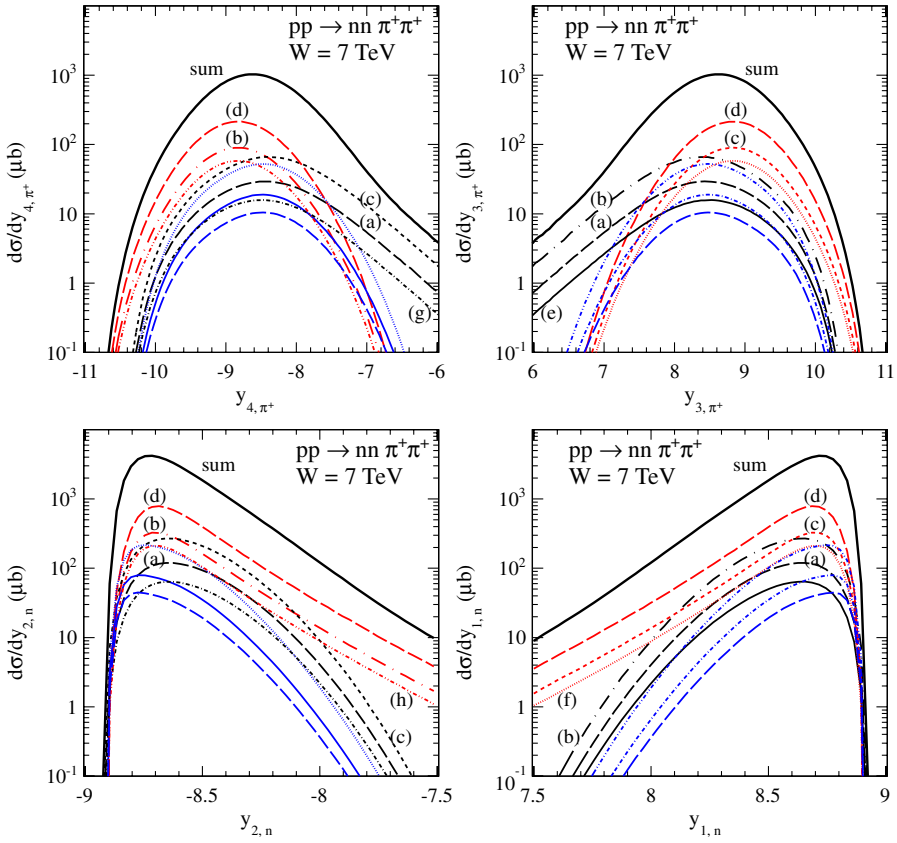

FIG. 6 (color online). Differential cross sections $d\sigma/dy_{\pi^+}$ and $d\sigma/dy_n$ at $W = 7$ TeV. The bold solid line represents the coherent sum of all amplitudes. The long-dashed (black), long-dash-dotted, dashed, long-dashed (red online), dash-dot-dot-dotted, dotted, dash-dotted, dash-dot-dotted, long-dashed (blue online) lines correspond to contributions from a)—i) diagrams. The red, black and blue lines correspond to diagrams when neutron, pion and proton are off-mass-shell, respectively. No absorption effects were included here.

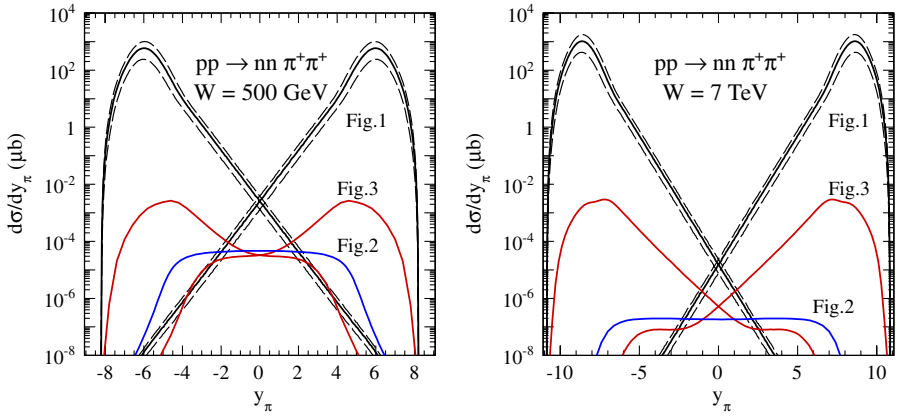

FIG. 7 (color online). Differential cross sections $d\sigma/dy_{\pi^+}$ at $W = 500$ GeV (left) and $W = 7$ TeV (right). The lines represent the coherent sum of all amplitudes from diagrams in Fig. 1–3, as well as separate classes of contributions marked by the number of the figure where they are shown. No absorption effects were included here.

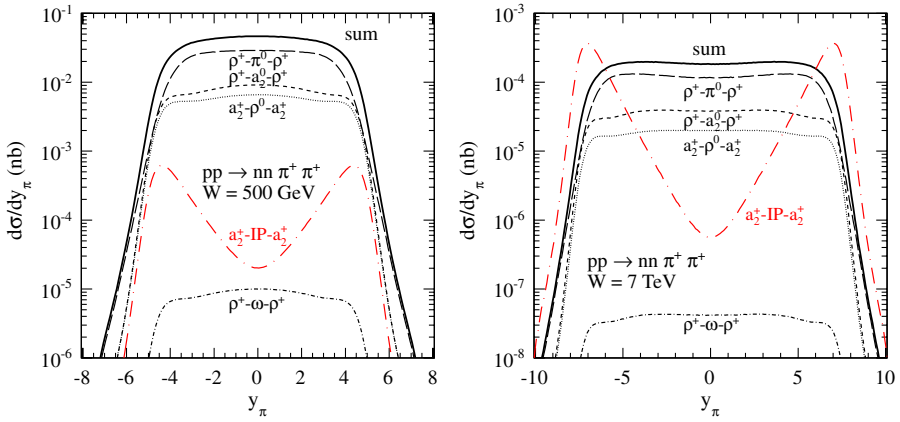

FIG. 8 (color online). Differential cross sections $d\sigma/dy_\pi$ for double-charged Reggeon exchanges at $W = 500$ GeV (left) and $W = 7$ TeV (right). The contributions for individual diagrams in Fig. 2 are shown separately. No absorption effects were included here.

of rapidities. The cross section corresponding to this mechanism is bigger by 2 orders of magnitude for the RHIC energy compared to the LHC energy, but rather small compared to the dominant contributions shown in Fig. 1. In addition, we show contribution of diagrams of Fig. 3. They are comparable to those of diagrams shown in Fig. 2 at midrapidities, but much smaller than those from Fig. 1 at larger rapidities. We show results of diagrams from Fig. 1 with different values of the form factor parameter $\Lambda = 0.8$ GeV (bottom dashed line) and $\Lambda = 1.2$ GeV (upper dashed line) in order to demonstrate the cross section uncertainties.

In Fig. 8, we present rapidity distributions of pions y_π for double-charged Reggeon exchanges at $W = 500$ GeV (left panel) and $W = 7$ TeV (right panel). The bold solid line represent the coherent sum of all amplitudes corresponding to diagrams in Fig. 2. The contributions for individual diagrams are also shown separately. The diagram in Fig. 2(a) gives the largest contribution (long-dashed line). The $a_2^+ - IP - a_2^+$ exchange corresponds to the long-dashed-dotted line. One can see that the double-Reggeon exchange mechanisms shown in Fig. 2 populate midrapidities of the pions and therefore can be measured either at RHIC or at LHC. In Table IV, we have collected cross section for this component separately for

TABLE IV. Full-phase-space integrated cross section (in nb) for exclusive $\pi^+\pi^+$ production for the amplitude with the double-charged Reggeon exchanges (diagrams in Fig. 2) at the center-of-mass energies $W = 0.5$, 7 TeV. No absorption effects were included here. The meaning of the acronyms: DSC—double spin-conserving, SSF—single spin-flip, DSF—double spin-flip.

exchange	$W = 0.5$ TeV	$W = 7$ TeV
$\rho^+ - \pi^0 - \rho^+$	0.43	3.3×10^{-3}
$\rho^+ - a_2^0 - \rho^+$	0.14	1.0×10^{-3}
$a_2^+ - \rho^0 - a_2^+$	0.11	5.4×10^{-4}
$\rho^+ - \omega - \rho^+$	1.5×10^{-4}	1.1×10^{-6}
sum of all amplitudes	0.7	5.1×10^{-3}
DSC	0.17	1.5×10^{-3}
SSF	0.18	1.3×10^{-3}
DSF	0.18	1.0×10^{-3}
$a_2^+ - IP - a_2^+$	4.4×10^{-3}	2.5×10^{-3}

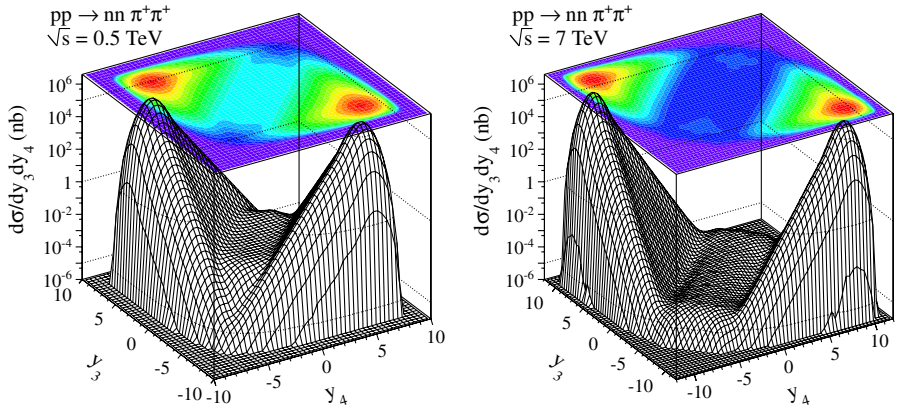

FIG. 9 (color online). Differential cross sections in (y_3, y_4) space at $W = 500$ GeV (left) and $W = 7$ TeV (right). The coherent sum of all amplitudes from diagrams in Fig. 1 and 3, and the contribution of diagrams in Fig. 2 with double-exchange Reggeons placed along the diagonal are presented. No absorption effects were included here.

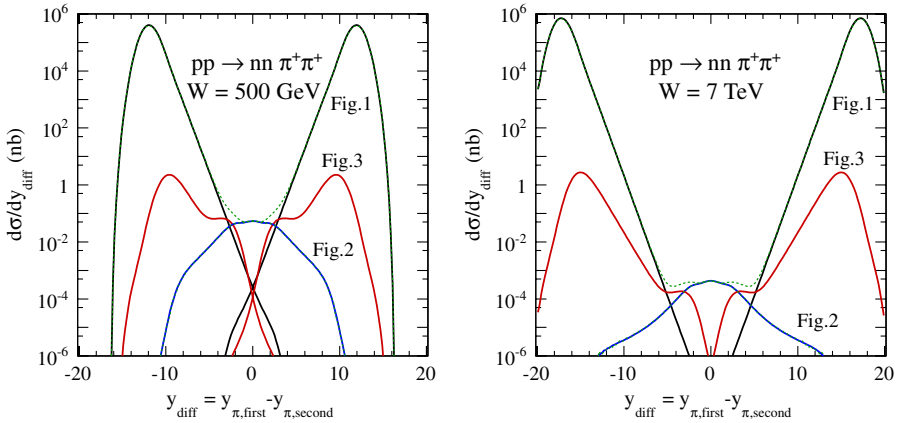

FIG. 10 (color online). Differential cross sections $d\sigma/dy_{\rm diff}$ at $W = 500$ GeV (left) and $W = 7$ TeV (right). The lines represent the coherent sum of all amplitudes from diagrams in Fig. 1 and 3, and the contribution of diagrams in Fig. 2 with double-exchange Reggeons placed at $y_{\rm diff} \approx 0$. No absorption effects were included here.

double spin-conserving (DSC), single spin-flip (SSF) and double spin-flip (DSF) contributions. All these spin contributions are of similar size. The total contribution is about half of nb at RHIC (500 GeV) and a few pb at LHC (7 TeV).

Can the much smaller contribution of diagrams with subleading-charged Reggeon exchanges be identified experimentally? In Fig. 9, we show two-dimensional distribution in (y_3, y_4) space. Thedouble-charged Reggeon-exchange components from Fig. 2 are placed along the diagonal $y_3 = y_4$ while the other contributions are some distance from the diagonal. Therefore, imposing two-dimensional cuts in the (y_3, y_4) space one could separate the small double-charged Reggeon contribution. A very good one-dimensional observable which can be used for the separation of the processes under discussion could be differential cross section $d\sigma/dy_{diff}$, where $y_{diff} = y_3 - y_4$ and experimentally charged pions should be taken at

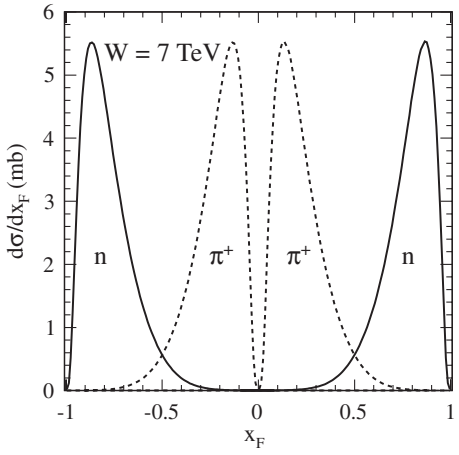

FIG. 11. Differential cross section $d\sigma/dx_F$ for the $pp \to nn\pi^+\pi^+$ reaction at $W = 7$ TeV. No absorption effects were included here.

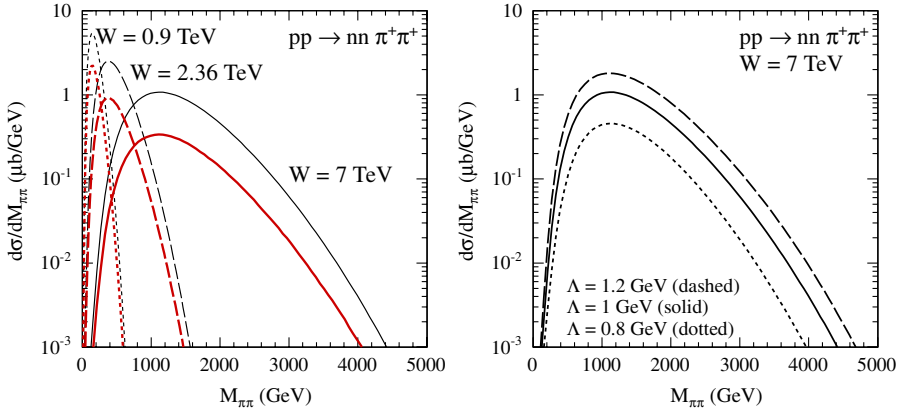

FIG. 12 (color online). Differential cross section $d\sigma/dM_{\pi\pi}$ for the $pp \to nn\pi^+\pi^+$ reaction at $W = 0.9, 2.36, 7$ TeV (left panel). The lower curves correspond to calculations with absorption effects. Right panel shows "bare" cross section obtained with different values of the form factor parameter $\Lambda = 0.8$ GeV (dotted line), $\Lambda = 1$ GeV (solid line) and $\Lambda = 1.2$ GeV (dashed line) at $W = 7$ TeV.

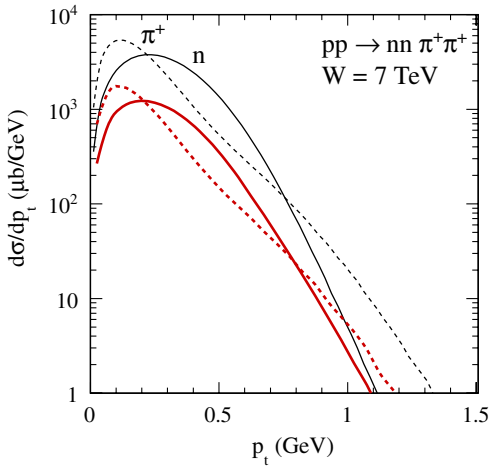

FIG. 13 (color online). Differential cross section $d\sigma/dp_t$ for the $pp \to nn\pi^+\pi^+$ reaction at $W = 7$ TeV. The solid and dotted lines correspond to the distribution in the transverse momentum of neutrons and pions, respectively. The lower curves correspond to calculations with absorption effects.

random (see Fig. 10, $y_{\pi,\text{first}} = y_3$ or y_4 and $y_{\pi,\text{second}} = y_4$ or y_3). For comparison, we show the contribution of diagrams in Fig. 3.

In Fig. 11, we show distribution of neutrons and pions in the Feynman variable $x_F = 2p_\parallel/\sqrt{s}$. In this observable, the neutrons and pions are well separated. The position of peaks is almost independent of energy. While pions are produce at relatively small x_F, the neutrons carry large fractions of the parent protons. The situation is qualitatively the same for all energies.

The distribution in pion-pion invariant mass is shown in Fig. 12. Unique for this reaction, very large two-pion invariant masses are produced (see e.g. Ref. [21]). The larger the energy, the larger the two-pion invariant masses (left panel). The absorption effects almost uniformly reduce the cross section. We show also distributions with different values of the form factor parameter in order to demonstrate the cross section uncertainties (righ panel).

The distributions in the transverse momentum of neutrons and pions are shown in Fig. 13. The figure shows that the typical transverse momenta are rather small but large

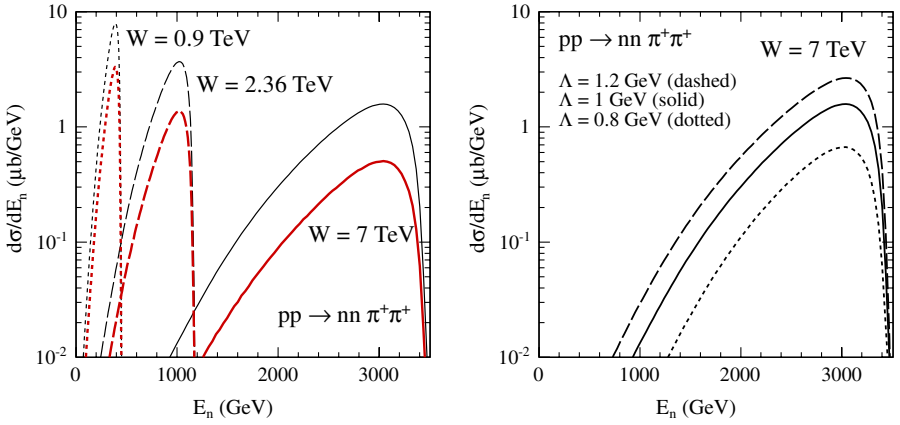

FIG. 14 (color online). Differential cross section $d\sigma/dE_n$ for the $pp \to nn\pi^+\pi^+$ reaction at $W = 0.9, 2.36, 7$ TeV (left panel). The lower curves correspond to calculations with absorption effects. Right panel shows bare cross section obtained with different values of the form factor parameter $\Lambda = 0.8$ GeV (dotted line), $\Lambda = 1$ GeV (solid line) and $\Lambda = 1.2$ GeV (dashed line) at $W = 7$ TeV.

enough to be measured. The distributions for neutrons are rather similar to those for pions.

The energy distributions of neutrons are presented in Fig. 14. Generally, the larger the collision energy, the larger the energy of outgoing neutrons. When combined with the previous plot, it becomes clear that the neutrons are produced at very small polar angles (large pseudorapidities) and can be measured by the ZDC's (see also Fig. 5).

In Fig. 15, we show two-dimensional correlations between energies of neutrons measured in both ZDC's. The figure shows that the energies of both neutrons are almost not correlated, i.e. the shape (not the normalization) of $d\sigma/dE_{n_1}$ ($d\sigma/dE_{n_2}$) is almost independent of E_{n_2} (E_{n_1}). There should be no problem in measuring energy spectra of neutrons on both sides as well as two-dimensional correlations in (E_{n_1}, E_{n_2}).

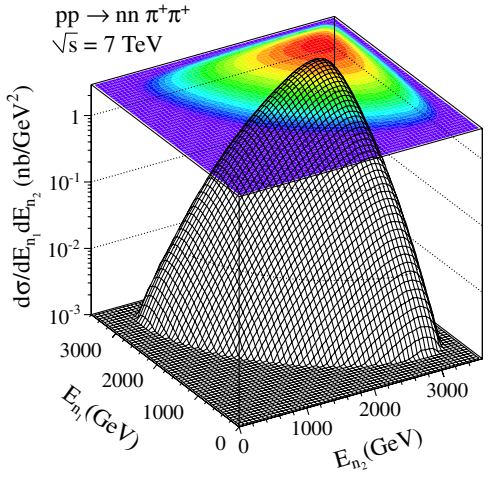

FIG. 15 (color online). Differential cross section $d\sigma/dE_{n_1}dE_{n_2}$ for the $pp \to nn\pi^+\pi^+$ reaction at $W = 7$ TeV.

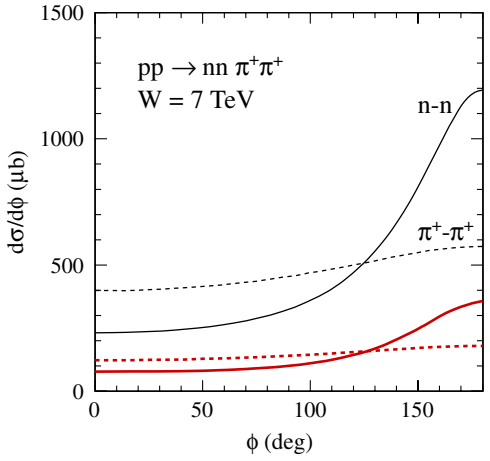

FIG. 16 (color online). Azimuthal angle correlations between neutrons and beetwen pions for the $pp \to nn\pi^+\pi^+$ reaction at $W = 7$ TeV. The lower curves correspond to calculations with absorption effects included.

TABLE V. Cross section (no absorption effects) with different experimental cuts on $p_{t,\pi}$, η_π and η_n.

	W (TeV)	$p_{t,\pi}>$	$\lvert\eta_\pi\rvert<$	$\lvert\eta_n\rvert_{ZDC}>$	σ (nb)
ALICE	7	0.15	0.9	8.7	6.3×10^{-5}
ALICE	7	0.15	1.2	8.7	1.2×10^{-4}
ATLAS	7	0.5	2.5	8.3	4.9×10^{-4}
CMS	7	0.75	2.4	8.5	4.5×10^{-4}
RHIC	0.5	0.2	1	—	2.0×10^{-2}

Finally, in Fig. 16, we present the distributions in azimuthal angle ϕ between the transverse momenta of the outgoing neutrons (pions). Clearly, a preference for back-to-back emissions can be seen. The measurement of azimuthal correlations of neutrons will be not easy with the first version of ZDC's, as only horizontal position can be measured. Still, correlations of horizontal hit positions on both sides could be interesting. A new correlation observable, taking into account possibilities of the apparatus, should be proposed. In contrast, the two π^+'s are almost not correlated in azimuthal angle. However, such a distribution may be not easy to measure.

We have shown that, at present, the reaction under consideration can be strictly measured only in a rather limited part of the phase space (midrapidities of pions), where the cross section is rather small and where the double-charged Reggeon mechanism dominates. In Table V we have collected the cross sections in nb for different experiments at LHC and RHIC. At LHC, where the separation of the double-Reggeon exchange mechanism is possible, the cross section is rather small—of the order of a fraction of pb. At RHIC, the cross section with experimental cuts should be easily measurable as it is of the order of a fraction of nb.

IV. CONCLUSIONS

We have estimated cross sections and calculated several differential observables for the exclusive $pp \to nn\pi^+\pi^+$ reaction. Because our parameters are extracted from the analysis of known two-body reactions we expect that our predictions of the cross section are fairly precise, in spite of the complications of the reaction mechanism. The full amplitude was parametrized in terms of leading Pomeron and subleading Reggeon trajectories. We have to consider three classes of diagrams. The first class gives the largest contribution but is concentrated at forward or backward pion directions. There are also diagrams with double-charged exchanges with subleading Reggeons ρ^+ and a_2^+. Although the cross section for these contributions is rather small, it is concentrated at midrapidities of pions where the

cross section can be easily measured. The double-exchange Reggeons processes can be separated out into the two-dimensional space of rapidities of both pions or in the distribution of the pion rapidity difference.

Large cross sections have been obtained, even bigger than for the $pp \to pp\pi^+\pi^-$ reaction [21]. Several mechanisms contribute to the cross section, which leads to an enhancement of the cross section due to interference effects. These interference effects cause that the extraction of the elastic $\pi^+\pi^+$ cross section as proposed recently seems in practice rather impossible.

The specificity of the reaction is that both neutrons and pions are emitted in very forward/backward directions, producing a huge rapidity gap at midrapidities. While the neutrons could be measured by the ZDC's, the identification of pions may be difficult. We think that the measurement of both neutrons and observation of large rapidity gap is a very good signature of the considered reaction. We expect the cross section for the $nn\pi^+\pi^+\pi^0$, $nn\pi^+\pi^+\pi^0\pi^0$, etc., which could destroy rapidity gaps, to be smaller but relevant estimates need to be done. In addition, for events with larger number of pions, the rapidity gap would be destroyed. Therefore, the formally kinematically incomplete measurement of two neutrons could be only relatively precise. We have found that the neutrons measured in ZDC's seem to be almost uncorrelated in energies.

We have made predictions for azimuthal angle correlations of outgoing neutrons. Such distribution should be possible to measure in a future. At present at CMS, only horizontal position can be measured. We have predicted back-to-back correlations with a sizeable diffusion.

We have included elastic rescattering effects in a way used recently for the three-body processes. These effects lead to a substantial damping of the cross section. The bigger the energy, the larger the effect of damping. Other processes (e.g. inelastic intermediate states or final state $\pi^+ n$ interactions) could lead to additional damping. At present there is no full understanding of the absorption effects. A future experiment could provide new data to be analyzed and could shed new light on absorption effects which are essential for understanding exclusive processes, even such important ones as exclusive production of the Higgs boson.

In the light of our analysis, it becomes clear that extraction of the elastic $\pi^+\pi^+$ cross section seems impossible, due to interference of several processes discussed in our paper. We did not find any corner of the phase space where the relevant diagram dominates.

There is an attempt to install forward shower counters in the LHC tunnel. Most probably they will not be able to measure energy of the pions but they can signal some activity there. We expect that ''some activity'' will mean, with a high probability, just one π^+ on one side and the other π^+ on the other side.

ACKNOWLEDGMENTS

We are indebted to Michael Murray for an interesting discussion on a possibility of a measurement of the discussed reaction and to Wolfgang Schäfer for a discussion of the reaction mechanisms. This study was partially supported by the Polish grant of MNiSW No. N202 249235.

APPENDIX

The ρ-meson/Reggeon and a_2-meson/Reggeon exchanges are known to have not only the nucleon spin-conserving part but also the dominant nucleon spin-flip component while the ω-meson/Reggeon exchange to nucleons is mainly spin-conserving. We write the amplitude for the Reggeon exchanges (see Fig. 17) in the following compact phenomenological form[5]:

$$\begin{aligned}\mathcal{M}^{\text{reggeon}-\text{exch.}}_{\lambda_N\to\lambda_{N'},\lambda_M}(s,t) &= \frac{\sqrt{-(t-t_{\min})}}{M_0}\left(\frac{-(t-t_{\min})}{4m_N^2}\right)^{|\lambda_{N'}-\lambda_N|/2} r_T^{i|\lambda_{n'}-\lambda_n|} \\ &\times \eta_i s C_i^r \left(\frac{s}{s_0}\right)^{\alpha_i(t)-1} \exp\left(\frac{B_{MN}}{2}(t-t_{\min})\right)\delta_{|\lambda_M|1},\end{aligned} \tag{A1}$$

and the pion exchange amplitude as

$$\begin{aligned}\mathcal{M}^{\pi-\text{exch.}}_{\lambda_N\to\lambda_{N'},\lambda_\rho}(s,t) &= g_{\pi NN}F_{\pi NN}(t)\bar{u}(p_{N'},\lambda_{N'})\mathrm{i}\gamma_5 u(p_N,\lambda_N) \\ &\times (k_\pi^\mu + q^\mu)\epsilon^*_\mu(k',\lambda_\rho)\frac{\mathrm{i}}{t-m_\pi^2} \\ &\times g_{\rho\pi\pi}F_{\rho\pi\pi}(t)\left(\frac{s}{s_0}\right)^{\alpha_\pi(t)}.\end{aligned} \tag{A2}$$

The $\sqrt{-(t-t_{\min})}/M_0$ factor above is due to the meson spin-flip (in the $\pi \to \omega$, $\pi \to \rho$ and $\pi \to a_2$ transitions), M_0 is a reference scale factor taken here $M_0 = 1$ GeV (which is used here to have the same units for the coupling constants). The double spin-flip components do not interfere with the spin-conserving ones and can be calculated separately. Here we have introduced one more phenomenological (dimensionless) parameter r_T^i, which describes coupling for the spin-flip components. It is known to be of $r_T^\rho = 7.5$, $r_T^{a_2} \simeq 6.14$, $r_T^\omega \simeq 0.17$[23] and $r_T^\rho \simeq 8$, $r_T^{a_2} \simeq 4.7$, $r_T^\omega \simeq 0.9$ [24]. In the present calculations we take $r_T^\rho = 7.5$, $r_T^{a_2} = 6$ and $r_T^\omega = 0$. The coupling constant $g_{\rho\pi\pi}$ is taken as $g^2_{\rho\pi\pi}/4\pi = 2.6$. The form factors are parametrized as $F(t) = \exp((t-m_\pi^2)/\Lambda^2)$. We improve the parametrization of the amplitude(A2) by multiplying by the factor $(s/s_0)^{\alpha_\pi(t)}$, where $\alpha_\pi(t) = \alpha'_\pi(t-m_\pi^2)$ is the pion Regge trajectory with the slope of trajectory $\alpha'_\pi = 1$ GeV^{-2}.

[5]For the case of the $\pi^- p \to \omega^0 n$, $\pi^- p \to \rho^0 n$ and $\pi^- p \to a_2^0 n$ reactions, the amplitude should be multiplied by $\sqrt{2}$, which is relatad to isospin Clebsch-Gordon coefficient.

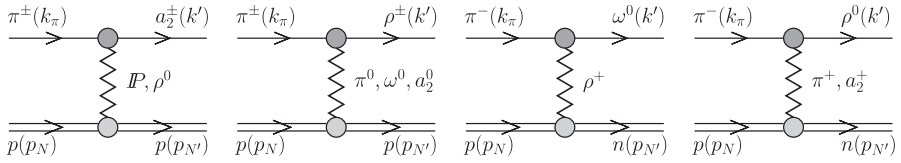

FIG. 17. Diagrams for various exchanges in πp collisions.

We adjust the C_i^r (where $i = IP,\ \rho,\ \omega,\ a_2$) coupling constants to the world experimental data often obtained from partial wave analysis in the three-pion system. The effective normalization constants for the auxiliary reactions are related to those in the NN scattering and the $g^i_{\pi\to a_2,\rho,\omega}$ coupling constants we need in our problem as

$$C_i^r = \sqrt{C_i^{NN}} \cdot g^i_{\pi\to j}. \tag{A3}$$

Since C_i^{NN} are known from phenomenology (Table I), $g^i_{\pi\to j}$ can be obtained from our fits: $g^{IP}_{\pi\to a_2} = 1.4\ \mathrm{GeV}^{-1}$, $g^{a_2}_{\pi\to\rho} = g^{a_2}_{\pi\to a_2} = 22\ \mathrm{GeV}^{-1}$ and $g^{\omega}_{\pi\to\rho} = g^{\rho}_{\pi\to\omega} = 4\ \mathrm{GeV}^{-1}$.

In Fig. 18, we show the total cross section for the $\pi^- p \to a_2^- p$, $\pi^- p \to \omega^0 n$, $\pi^- p \to \rho^0 n$ and $\pi^\pm p \to \rho^\pm p$ reactions as a function of the incident-beam momenta P_{lab}. Our fit is shown by the solid line. In the panel a) ($\pi^- p \to a_2^- p$ reaction), we show individual contributions of ρ and Pomeron exchanges. The Pomeron exchange dominates at high energies whereas the ρ exchange at small energies. This separation of mechanisms allows to extract two independent coupling constants. We show also spin-conserving and spin-flip amplitudes separately. In panel b), we show our fit for the $\pi^- p \to \omega^0 n$. Here only ρ exchange is possible. In panel c) ($\pi^- p \to \rho^0 n$ reaction), we show contributions for charged pion exchange (parameters fixed from phenomenology) and a_2 exchange (parameters found from the analysis of the $\pi^- p \to a_2^- p$ (see panel a))). Finally, in panel d) ($\pi^\pm p \to \rho^\pm p$ reactions), we show contributions for neutral pion exchange, a_2 exchange and ω exchange (relevant coupling constant found from the analysis of the $\pi^- p \to \omega^0 n$ reaction (see panel b))).

Having fixed the parameters, we can proceed to our four-body $pp \to nn\pi^+\pi^+$ reaction.

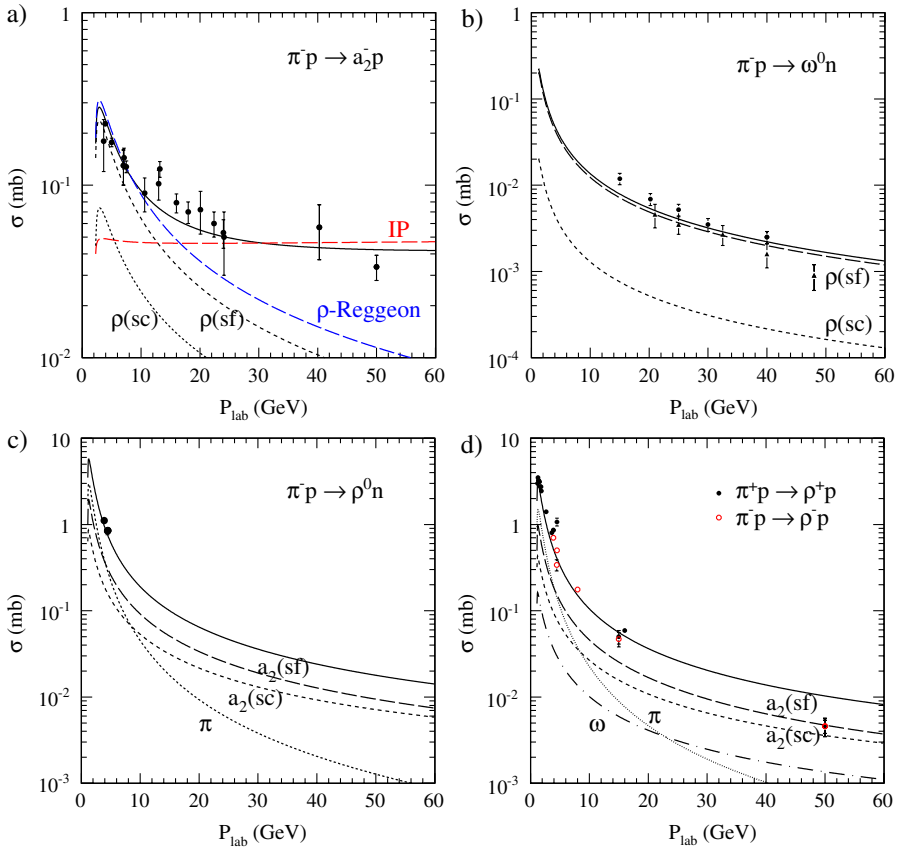

FIG. 18 (color online). The integrated cross section for the $\pi^- p \to a_2^- p$ (the experimental data are taken from [26,27]), $\pi^- p \to \omega^0 n$ [28], $\pi^- p \to \rho^0 n$ [29,30], $\pi^+ p \to \rho^+ p$[27,30–32] and $\pi^- p \to \rho^- p$[27,29–31,33] reactions as a function of the incident-beam momenta P_{lab}.

[1] K. Nakamura (Particle Data Group), J. Phys. G **37**, 075021 (2010).

[2] V. A. Petrov, R. A. Ryutin, and A. E. Sobol, Eur. Phys. J. C **65**, 637 (2009).

[3] A. E. Sobol, R. A. Ryutin, V. A. Petrov, and M. Murray, Eur. Phys. J. C **69**, 641 (2010).

[4] A. Grau, G. Pancheri, O. Shekhovtsova, and Y. N. Srivastava, Phys. Lett. B **693**, 456 (2010) .

[5] M. G. Albrow (FP420 Collaboration), JINST **4** T10001 (2009) , The FP420 R&D project: Higgs and new physics with forward protons at the LHC, http://www.iop.org/EJ/abstract/1748-0221/4/10/T10001.

[6] O. A. Grachov (CMS Collaboration), J. Phys. Conf. Ser. **160**, 012059 (2009).

[7] M. Murray, ''Forward neutrons in CMS,'' at ECT Trento workshop, Trento, January 4-8, 2010.

[8] J. Peter (ATLAS Collaboration), No. CERN-LHCC-2007-001, No. LHCC-I-016, http://cdsweb.cern.ch/record/1009649.

[9] P. D. B. Collins, *An Introduction to Regge Theory and High-Energy Physics* (Cambridge University Press, Cambridge, England, 1977); S. Donnachie, G. Dosch, P. Landshoff, and O. Nachtmann, *Pomeron Physics and QCD* (Cambridge University Press, Cambridge, England, 2002).

[10] W. Schäfer and A. Szczurek, Phys. Rev. D **76**, 094023 (2007).

[11] G. Alberi and G. Goggi, Phys. Rep. **74**, 1 (1981).

[12] A. Szczurek and P. Lebiedowicz, Nucl. Phys. **A826**, 101 (2009).

[13] A. Szczurek, N. N. Nikolaev, and J. Speth, Phys. Rev. C **66**, 055206 (2002).

[14] P. Lebiedowicz, A. Szczurek, and R. Kamiński, Phys. Lett. B **680**, 459 (2009).

[15] T. E. O. Ericson, B. Loiseau, and A. W. Thomas, Phys. Rev. C **66**, 014005 (2002).

[16] H. Holtmann, N. N. Nikolaev, A. Szczurek, J. Speth, and B. G. Zakharov, Z. Phys. C **69**, 297 (1996).

[17] Z. Ouyang, J. J. Xie, B. S. Zou, and H. S. Xu, Int. J. Mod. Phys. E **18**, 281 (2009); Xu Cao, B. S. Zou, and H. S. Xu, Phys. Rev. C **81** 065201 (2010) .

[18] A. Donnachie and P. V. Landshoff, Phys. Lett. B **296**, 227 (1992).

[19] R. Machleidt, K. Holinde, and Ch. Elster, Phys. Rep. **149**, 1 (1987); D. V. Bugg and R. Machleidt, Phys. Rev. C **52**, 1203 (1995).

[20] A. Szczurek and J. Speth, Nucl. Phys. **A555**, 249 (1993); B. C. Pearce, J. Speth, and A. Szczurek, Phys. Rep. **242**, 193 (1994); J. Speth and A. W. Thomas, Adv. Nucl. Phys. **24**, 83 (2002).

[21] P. Lebiedowicz and A. Szczurek, Phys. Rev. D **81**, 036003 (2010).

[22] V. A. Khoze, A. D. Martin, and M. G. Ryskin, Eur. Phys. J. C **18**, 167 (2000); U. Maor, AIP Conf. Proc. **1105**, 248 (2009).

[23] G. L. Kane and A. Seidl, Rev. Mod. Phys. **48**, 309 (1976).

[24] A. C. Irving and R. P. Worden, Phys. Rep. **34C**, 117 (1977).

[25] C. Adler *et al.*, Nucl. Instrum. Methods Phys. Res., Sect. A **470**, 488 (2001).

[26] A. C. Irving, Nucl. Phys. **B121**, 176 (1977); A. Ferrando *et al.*, Nucl. Phys. **B135**, 237 (1978); J. A. Gaidos *et al.*, Phys. Rev. D **19**, 22 (1979).

[27] A. Delfosse *et al.*, Nucl. Phys. **B183**, 349 (1981).

[28] V. N. Bolotov, Yad. Fiz. **21**, 316 (1975); Sov. J. Nucl. Phys. **21**, 166 (1975); W. D. Apel (Serpukhov-CERN Collaboration), Yad. Fiz. **31**, 167 (1980); Lett. Nuovo Cimento Soc. Ital. Fis. **25**, 493 (1979).

[29] A. A. Kartamyshev *et al.*, Yad. Fiz. **15**, 294 (1972).

[30] B. Haber *et al.*, Phys. Rev. D **10**, 1387 (1974); E. A. Alekseeva *et al.*, Zh. Eksp. Teor. Fiz. **82**, 1007 (1982); Sov. Phys. JETP **55**, 591 (1982).

[31] J. C. Pratt *et al.*, Phys. Lett. B **41**, 383 (1972).

[32] P. L. Bastien *et al.*, Phys. Rev. D **3**, 2047 (1971); W. Michael and G. Gidal, Phys. Rev. Lett. **28**, 1475 (1972); Y. Williamson *et al.*, Phys. Rev. Lett. **29**, 1353 (1972); A. Berthon *et al.*, Nucl. Phys. **B81**, 431 (1974); M. Deutschmann *et al.*, Nucl. Phys. **B86**, 221 (1975); **B103**, 547(E) (1976); J. Macnaughton *et al.*, Phys. Rev. D **15**, 1832 (1977).

[33] W. M. Bugg *et al.*, Phys. Rev. D **26**, 2183 (1982).